Intraband and intersubband many-body effects in the nonlinear optical response of single-wall carbon nanotubes

Benjamin Langlois,[1] Romain Parret,[1] Fabien Vialla,[1] Yannick Chassagneux,[1] Philippe Roussignol,[1] Carole Diederichs,[1] Guillaume Cassabois,[2] Jean-Sébastien Lauret,[3] and Christophe Voisin[1,*]

[1]*Laboratoire Pierre Aigrain, École Normale Supérieure, Université Paris Diderot, UPMC, CNRS UMR8551, 24 rue Lhomond, 75005 Paris, France*
[2]*Laboratoire Charles Coulomb, Université Montpellier, CNRS UMR5221, 34095 Montpellier, France*
[3]*Laboratoire Aimé Cotton, ENS Cachan, CNRS, Université Paris Sud, 91405 Orsay, France*

We report on the nonlinear optical response of a monochiral sample of (6,5) single-wall carbon nanotubes by means of broadband two-color pump-probe spectroscopy with selective excitation of the S_{11} excitons. By using a moment analysis of the transient spectra, we show that all the nonlinear features can be accurately accounted for by elementary deformations of the linear absorption spectrum. The photogeneration of S_{11} excitons induces a broadening and a blueshift of both the S_{11} and S_{22} excitonic transitions. In contrast, only the S_{11} transition shows a reduction of oscillator strength, ruling out population up-conversion. These nonlinear signatures result from many-body effects, including phase-space filling, wave-function renormalization, and exciton collisions. This framework is sufficient to interpret the magnitude of the observed nonlinearities and stress the importance of intersubband exciton interactions. Remarkably, we show that these intersubband interactions have the same magnitude as the intraband ones and bring the major contribution to the photobleaching of the S_{22} excitonic transition upon S_{11} excitation through energy shift and broadening.

PACS number(s): 73.63.Fg, 78.47.D−

I. INTRODUCTION

Single-wall carbon nanotubes are unique nearly one-dimensional nanostructures that trigger a wealth of investigations regarding both academic aspects and applications. The possible geometries of these hollow cylinders, known as chiral species, give rise to a large variety of electronic properties that are uniquely related to their structure [1]. The electronic and optical properties of carbon nanotubes reflect large electronic correlations leading, for instance, to the formation of strongly bound excitons, even at room temperature [2,3]. At higher excitation densities, electronic correlations give rise to a number of new signatures related to the exciton-exciton interactions, including exciton-exciton annihilation [4] or the formation of biexcitons [5] or trions [6] below the S_{11} excitonic transition. These nonlinear effects are already successfully exploited for applications as saturable absorbers in ultrafast lasers, for instance [7]. In contrast to other semiconducting nanostructures, the magnitude of these interactions is strongly enhanced by the one-dimensional geometry of the nanotubes [8]. Besides excitonic complexes and exciton annihilation, many-body effects also induce broad spectral range optical signatures such as band-gap renormalization or collisional broadening [9]. In contrast to excitonic complexes, such effects are best detectable at photon energies larger than that of the lower excitonic transition.

In most of the previous studies, however, such effects were blurred because of the spectral congestion of optical transitions due to the use of polychiral suspensions [10,11]. As a consequence, most of the previous pump-probe studies

have been interpreted in terms of simple photobleaching (PB) and photoabsorption (PA) bands respectively assigned to state filling effects (Pauli blocking in a molecular picture) and absorption from long-lived excited states to upper states [11–13]. This empirical approach to the nonlinear optical properties of carbon nanotubes suffers from two main issues: first, the molecular picture does not take properly into account the bosonic nature of the excitonic excitations, and secondly, the PA bands require the introduction of *ad hoc* upper states that are not supported by calculations of the electronic structure of the nanotubes.

In this study, we present a broad spectral range investigation of the optical nonlinearities in a monochiral ensemble of carbon nanotubes. We focus on the case of a low-energy (S_{11}) pumping scheme that is more suited to unveil many-body effects beyond simple phase-space filling effects. We use an intrinsic analysis method based on the moments of the transient absorption spectra that does not require any assumption about the line shape of the transitions. We show that the photocreation of S_{11} excitons induces a broadening and a blueshift of both the S_{11} and S_{22} lines of the order of a few meV. In contrast, the reduction of oscillator strength is observed only for the S_{11} transition, showing that strong changes in the S_{22} absorption band can be obtained through nonlinear intersubband interactions even if the S_{22} population remains negligible. Furthermore, by using combinations of nonlinear signals, we can eliminate the (unknown) exciton density and access in the most possible intrinsic way to the microscopic parameters. All these experimental observations can be accounted for in a simple and unified description of many-body effects in carbon nanotubes, based on a mean-field perturbative approach that generalizes to the one-dimensional case the calculations previously developed for two-dimensional nanostructures [14,15].

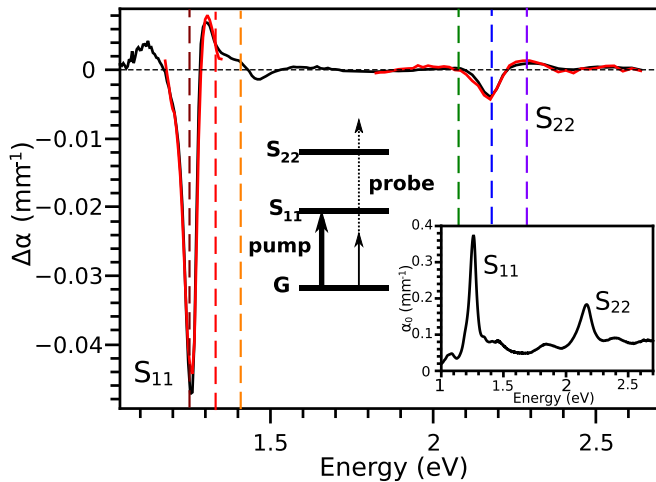---

*christophe.voisin@lpa.ens.fr

FIG. 1. (Color online) A broadband nonlinear absorption spectrum (black) 1 ps after S_{11} excitation at a fluence of 2×10^{13} photons cm^{-2}. Fit (red) of the data using a direct deformation (including reduction of oscillator strength, shift, and broadening) of the linear absorption spectrum. Probe energy references for Fig. 2 (vertical dashed lines). Inset: linear absorption spectrum.

FIG. 2. (Color online) Relaxation dynamics of normalized transient absorption after S_{11} excitation for probe energies given by the dashed vertical lines of Fig. 1 (same color code). The black dashed line corresponds to a $t^{-0.47}$ normalized decay. Inset: normalized nonlinear absorption spectra excited at 1.26 eV, fluence of 3.2×10^{14} photons cm^{-2}, for different pump-probe delays.

II. EXPERIMENTAL SETUP AND SAMPLES

The sample consists of an aqueous suspension of (6,5) enriched carbon nanotubes encapsulated in micelles purchased from NanoIntegris. The suspension is placed in a 1-mm-thick quartz cuvette for the measurements of both the linear and nonlinear properties. The linear absorption (α_0) spectrum is displayed in the inset of Fig. 1. It consists of two main lines at 1.25 and 2.2 eV corresponding to the excitonic transitions of the first and second subbands, respectively, the so-called S_{11} and S_{22} transitions. In addition to these main features, weaker resonances are attributed to phonon sidebands [16] and possibly remaining minority chiral species. Finally, these resonances lie on a flat absorption background attributed to both an intrinsic nonresonant contribution [17] and to various impurities [18]. We delineate those two contributions by means of a thorough comparison of the absorption spectrum with the photoluminescence excitation spectrum (PLE) of the same suspension, which allows us to access the truly intrinsic absorption of the (6,5) species [17] in the [1.4–3 eV] window.

The nonlinear signals are obtained from copolarized pump-probe measurements at a subpicosecond time scale. The pump-probe setup is based on a visible optical parametric amplifier (OPA) pumped at 400 nm by a frequency doubled amplified Ti:sapphire laser at a repetition rate of 250 kHz. Part of the continuum generated in a sapphire crystal to seed the OPA is picked up to serve as a probe beam, whereas the signal or idler beams of the OPA are used as a pump. The wavelength can be tuned continuously from 445 to 1200 nm (1 to 2.8 eV) with a spectral width of the order of 15 meV. In the following, the pump energy is fixed at 1.25 eV in resonance with S_{11}, except when otherwise specified. The probe beam is further filtered by a monochromator (5 nm bandpass) after passing through the sample [19]. The instrumental response of the setup was measured by stimulated Raman scattering in water and gives
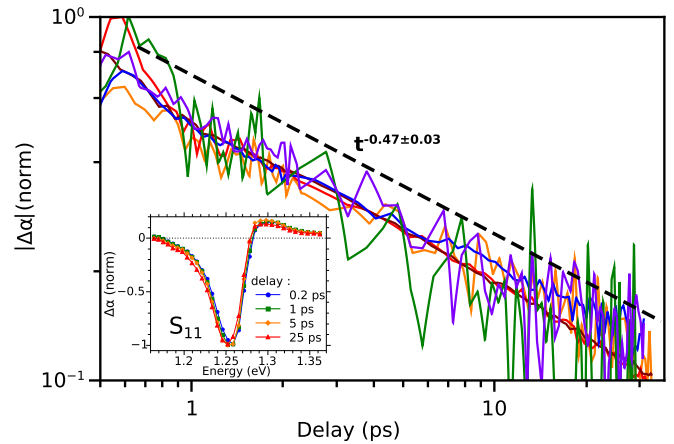
an overall temporal resolution of 270 fs. The chirp of the probe beam was measured and numerically corrected in the data.

III. TRANSIENT SPECTRA AND QUANTITATIVE ANALYSIS

The nonlinear broadband spectrum shown in Fig. 1 consists of photoabsorption ($\Delta\alpha > 0$) and photobleaching ($\Delta\alpha < 0$) bands near each excitonic resonance. The signal in the S_{22} spectral range is about ten times smaller than in the S_{11} range. The shape of the (normalized) nonlinear spectra does not depend on the pump-probe time delay (see inset of Fig. 2) or on the pump wavelength (as already reported in Ref. [13], for instance). Neither does it depend on the fluence except in the very first picoseconds after excitation at high fluence (above 10^{15} cm^{-2}).

In order to determine the origin of the nonlinear signal, we first focus on the relaxation dynamics of the transient absorption for different probe frequencies (Fig. 2). The relaxation of the transient absorption resonant with S_{11} is known to follow a $\Delta\alpha(t) \propto t^{-1/2}$ decay law from a few picoseconds up to 1 ns after excitation of either the S_{11} or S_{22} transitions [13,20], independently of the pump power [21]. Zhu *et al.* also showed that the transient absorption at S_{22} follows the same dynamics [13]. This decay is typical of a diffusion limited annihilation reaction between identical particles in a one-dimensional material [22,23]. In the case of carbon nanotubes, this relaxation is interpreted as exciton-exciton annihilation [13,21], which is known to be significant in strongly confined systems [24]. Figure 2 shows that the same dynamics is also observed in the nonresonant transient absorption on both sides of the excitonic transitions. The PB and PA bands clearly display the same relaxation dynamics, indicating that all nonlinear features stem from a unique physical origin, namely, the dynamics of the lower energy S_{11} excitations.

We now turn to the physical origin of these nonlinear signatures by investigating systematically the spectral shape of the transients. We achieve a simple and consistent description by considering a minimal set of many-body effects that is able to account for the nonlinear optical signatures on a very wide range of probe energies. These nonlinear signatures are interpreted as consequences of the presence of S_{11} excitons in the nanotube leading to phase-space filling, wave-function renormalization, and excitonic collisions. These effects reshape all the excitonic resonances and can be accounted for by elementary deformations of each excitonic line S_{ii}: reduction of oscillator strength Δf^{ii}, energy shift ΔE^{ii}, and broadening $\Delta\Gamma^{ii}$ with respect to the equilibrium values f_0^{ii}, E_0^{ii}, and Γ_0^{ii}.

In a first approach, elementary deformations are separately applied to the linear spectrum near S_{11} and S_{22} resonances in order to reproduce qualitatively the nonlinear spectra. This approach allows one to fully reproduce the experimental data as can be seen in Fig. 1 (red curves). Computing this nonlinear spectrum requires two precautions. First, the spectrum boundaries must be chosen so as to avoid extrinsic contributions such as the ones of minority chiral species that are not resonantly excited by the pump. Otherwise, the procedure would generate artifacts. Similarly, the influence of multiexcitonic complexes, which is well documented [5,25], has not been introduced, such complexes giving specific signatures below 1.1 eV in the case of (6,5) nanotubes. Secondly, the extrinsic absorption background has to be subtracted from the linear spectrum before applying any deformation in order to obtain a reliable simulated nonlinear spectrum. This background can be accurately evaluated from PLE measurements [17]. This background correction method, however, is not applicable near the S_{11} resonance due to overwhelming elastic scattering in the PLE spectrum. Nevertheless, the computed nonlinear spectrum successfully reproduces the PA and PB band profiles, especially their asymmetry and relative amplitudes. This indicates that the three elementary deformations considered in this description are sufficient to accurately reproduce the nonlinear spectra. Reciprocally, we note that all three of these contributions are necessary, except Δf^{22}. In fact, considering only a reduction of oscillator strength ($\Delta f < 0$) would produce a symmetric PB band, whereas a simple energy shift ΔE would give rise to a derivativelike profile composed of a pair of PB and PA bands of similar amplitude, and a plain broadening $\Delta\Gamma$ would lead to a PB band surrounded by two symmetrical PA bands.

In order to get a more quantitative insight into the many-body effects responsible for these nonlinear signatures, we now use the moment analysis technique. This method is particularly well suited to quantitatively determine the characteristics of a band of arbitrary shape [26] and is insensitive to most of the limitations mentioned above. The oscillator strength f_0^{ii}, the mean energy E_0^{ii}, and the width Γ_0^{ii} are defined, respectively, as the zeroth, first, and second moment of the linear absorption of the corresponding line. This method does not require any assumption regarding the line shape of the resonances, all the parameters being defined in an intrinsic way through integrals of the spectrum near the resonances. Practically, the oscillator strength reads $f_0^{ii} = \int_{\Delta E} \alpha_0^{ii}(E)dE/(\Delta E)$, the energy position of the resonance reads $E_0^{ii} = \int_{\Delta E} E\alpha_0^{ii}(E)dE/(f_0^{ii}\Delta E)$, and the width Γ_0^{ii}
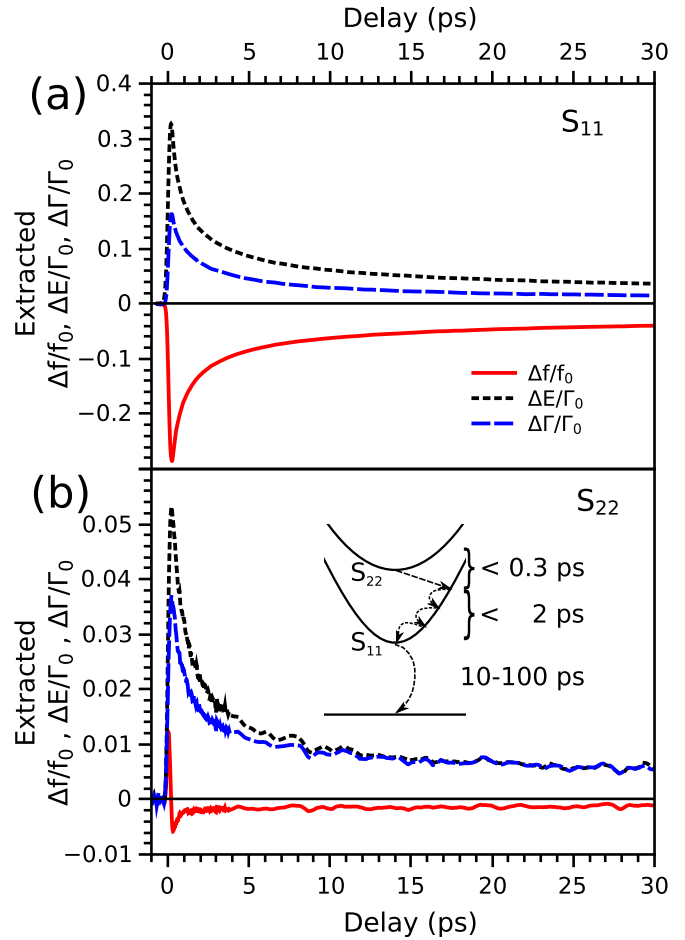

FIG. 3. (Color online) Relaxation dynamics of the elementary deformations of S_{11} (a) and S_{22} (b) bands with S_{11} excitation at a fluence of 3.2×10^{14} photons cm^{-2}.

is given by $(\Gamma_0^{ii})^2 = \int_{\Delta E}(E - E_0^{ii})^2\alpha_0^{ii}(E)dE/(f_0^{ii}\Delta E)$. Applied to the nonlinear spectra, this method gives access to the elementary deformations as a function of the time elapsed since excitation [Figs. 3(a) and 3(b)] according to

$$\Delta f^{ii}(t) = \frac{1}{\Delta E}\int_{\Delta E}\Delta\alpha^{ii}(E,t)dE$$

for the oscillator strength,

$$\Delta E^{ii}(t) = E^{ii}(t) - E_0^{ii}$$

with

$$E^{ii}(t) = \frac{1}{f_0^{ii}\Delta E}\int_{\Delta E}E\big[\alpha_0^{ii}(E) + \Delta\alpha^{ii}(E,t)\big]dE$$

for the energy shift, and

$$\Delta\Gamma^{ii}(t) = \Gamma^{ii}(t) - \Gamma_0^{ii}$$

with

$$[\Gamma^{ii}(t)]^2 = \frac{1}{f_0^{ii}\Delta E}\int_{\Delta E}[E - E^{ii}(t)]^2[\alpha_0(E) + \Delta\alpha^{ii}(E,t)]dE$$

for the broadening. We used an integration window of [1.16–1.36 eV] and [1.95–2.55 eV] for analyzing the nonlinear changes of the S_{11} and S_{22} transitions, respectively. Basically,
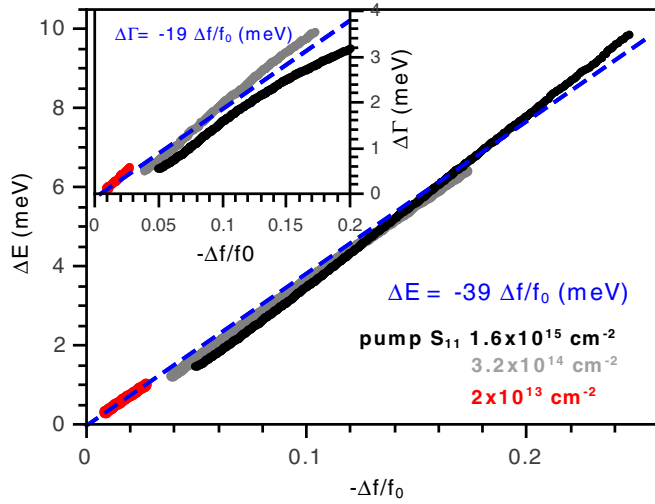
FIG. 4. (Color online) Energy shift and broadening (inset) of the S_{11} excitonic transition as a function of the change of oscillator strength of the same transition, extracted from the moment analysis (see text) for a resonant pumping of the S_{11} transition and for several excitation densities.

Fig. 3 shows that the three contributions to the S_{11} nonlinear spectra are of similar amplitude and thus are of equal importance to appropriately describe the nonlinear signals.

We first focus on the reduction of oscillator strength in each subband. Indeed, we shall see in the theoretical section (Sec. IV) that it fairly reflects the excitonic population of the same subband ($\Delta f^{ii} \propto n^{ii}$). In order to follow the excitonic population relaxation in the first and second subbands, we thus compare the dynamics of their respective Δf after excitation on S_{11} [Figs. 3(a) and 3(b)]. Strikingly, $\Delta f^{22}/f_0^{22}$ becomes completely negligible within a few picoseconds, whereas $\Delta f^{11}/f_0^{11}$ remains sizable for several tens of picoseconds. This means that the S_{22} population becomes negligible within a picosecond even though a small up-conversion from the S_{11} state can be seen in the very early delays. Note that the same ultrafast disappearance of the S_{22} population is observed upon direct pumping of the S_{22} transition or at higher energy (not shown), which confirms that the dynamics of the two types of excitons is very different, the upper one showing a much reduced lifetime [27,28]. We emphasize that the dynamics of Δf^{22} is quite singular as compared to the dynamics of the change of absorption of this band. This means that the bleaching of the S_{22} band originates from other processes than band filling. We end up with the picture that within a few picoseconds electron-hole pairs populating S_{11} states are predominant in the nanotube. The absence of S_{22} population after excitation by the pump pulse is consistent with calculations of exciton relaxation from S_{22} to S_{11} implying efficient TO- and LA-phonon emission in less than 300 fs [29] (inset of Fig. 3).

ΔE^{11} and $\Delta \Gamma^{11}$ are plotted against Δf^{11} in Fig. 4. The experimental values of the broadening are compatible with our previous studies using spectral hole-burning experiments [9], although the experimental conditions are quite different (chiral distribution, temperature, etc.) showing that these nonlinear properties are essentially intrinsic. As we shall see in Sec. IV, the energy shift and broadening naturally scale with the exciton binding energy E_b. Our study shows that $\Delta \Gamma^{11}/E_b = 0.05 \Delta f^{11}/f_0$ with $E_b = 350$ eV, which is consistent with the relation $\Delta \Gamma^{11}/E_b = [0.02 - 0.1]\Delta f^{11}/f_0$ obtained by Nguyen *et al.* [9]. We note that this previous study did not mention any spectral shift. This actually points out an important difference between the two methods. Spectral hole-burning experiments in an inhomogeneous distribution yield an average of the nonlinear signals over a spectral window equivalent to the homogeneous linewidth. In contrast to the oscillator strength reduction and to the broadening, the change of absorption due to an energy shift is an odd function with a vanishing average value. We actually estimated that in our previous (hole-burning) study the residual effect of a spectral shift would be at least one order of magnitude lower than the two other contributions [9] due to this averaging effect.

In contrast, in this chiral enriched sample showing little inhomogeneous broadening, we observe that the photoexcitation of carbon nanotubes consistently leads to a blueshift of the excitonic resonances. We note that such a blueshift of a few meV at high excitation is commonly observed in other semiconductor nanostructures (see, for instance, Refs. [26,30]). In the case of carbon nanotubes a blueshifted PA was reported in several studies for short time delays, whereas at longer time delays, transient spectra were tentatively interpreted with redshifts of the lines [8,10,13,31]. We do not observe such redshift in our data. This inconsistency in the literature is probably due to the use of polydisperse samples in several of these studies that prevented a fine identification of the spectral changes. As a consequence, the physical interpretation also remained quite elusive: these PA bands were tentatively assigned to transitions to the biexciton [10], to a speculative transition to the two-exciton S_{11} manyfold [13], to the Stark shift induced by photoinduced free carriers [31] or to the coupling with nonequilibrium hot phonons [8].

Finally, we observe a linear relationship between all the nonlinear quantities over time (Fig. 4), which clearly shows that they share the same dynamics, independently of the pump power, in agreement with a common physical origin. Quantitatively, this linear relationship reads $\Delta E^{11}(\mathrm{meV}) = -(39 \pm 5)\Delta f^{11}/f_0^{11}$. The broadening of the S_{11} resonance also presents a linear relationship with Δf^{11} (inset of Fig. 4): $\Delta \Gamma^{11}(\mathrm{meV}) = -(19 \pm 5)\Delta f^{11}/f_0^{11}$. Interestingly, Fig. 4 shows that despite a possibly complicated (multicomponent) time decay, the evolution of one of these parameters as a function of another shows a simple linear relationship over a large span (two orders of magnitude) of initial carrier density. This shows that the three parameters share the same exciton density dependence (cf. Sec. IV D).

IV. MODELING OF MANY-BODY EFFECTS

In order to connect the macroscopic nonlinear signatures Δf, ΔE, and $\Delta \Gamma$ to the underlying microscopic many-body effects, we developed a lowest order calculation of these effects by generalizing to the one-dimensional case the models established for two-dimensional nanostructures [14,15], which are based on a first order perturbative mean-field approach. From a qualitative point of view, these many-body effects can be split into two main contributions. The first one is the
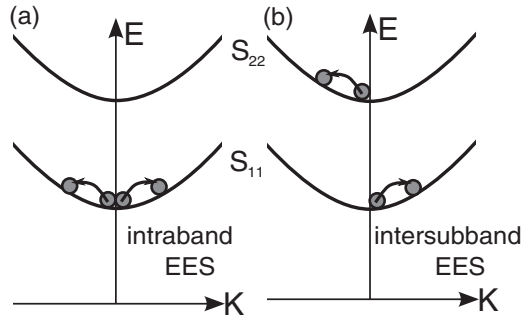
FIG. 5. Exciton energy dispersion and schematic representation of the quasielastic exciton-exciton scattering process for the intraband case (a) and intersubband case (b).

so-called phase-space filling (PSF) effect that is reminiscent of the Pauli principle acting on the fermionic components of the excitons (composite bosons). It mainly gives rise to a reduction of the oscillator strength Δf_{PSF}. The second one is related to the Coulomb interactions which give rise to several contributions, including short-range effects such as exchange interaction, direct interaction, or exciton wave-function renormalization (EWR) and long-range effects (screening).

The contribution of the direct Coulomb interaction vanishes in the particular case of carbon nanotubes because of the identical effective masses of conduction electrons and holes [32]. For two-dimensional nanostructures, the exchange of one fermion between two excitons gives rise to a blueshift as long as the momentum exchanged during the process is small as compared to the inverse of the excitonic Bohr radius [15,33]. In our experimental conditions, we therefore anticipate a blueshift due to this effect. The EWR results from the corrections to the exciton wave function when taking into account the Coulomb perturbation. It mainly redistributes the oscillator strength of the transition, giving an additional contribution Δf_{EWR}. Finally, the screening of the Coulomb interaction by the population of excitons gives corrections to all the previously mentioned terms, leading to an overall redshift. The screening by excitons is, however, much weaker than that due to free carriers, especially in the case of carbon nanotubes where the small Bohr radius of the exciton reduces considerably their polarizability [2]. Furthermore, it is well established that such screening is strongly suppressed in reduced dimensionality systems [14]. In a classical picture, this results from the impossibility for counter charges to surround the test charge. In the following, the effects of excitonic screening will be neglected. As a consequence, the calculated nonlinear effects shall be considered as upper bounds. Finally, we also take into account the broadening resulting from the interaction between the excitons belonging either to the same or to separate subbands. This broadening arises from both the direct exciton-exciton annihilation (EEA) processes that give rise to a lifetime reduction and from quasielastic exciton-exciton scattering (EES) within a given subband or across a pair of bands (Fig. 5).

In line with previous works, we use the contact interaction approximation to regularize the Coulomb interaction [Eq. (1)], which is justified by the very small Bohr radius in carbon nanotubes [24].

$$V_{contact} = -U\delta(r) \qquad (1)$$

with $U > 0$. The value of U is set by the scaling law with the exciton binding energy E_b, which is known from experiments [2,34].

$$E_b = \frac{\mu U^2}{2\hbar^2} = \frac{\hbar^2}{2\mu r_B^2}, \qquad (2)$$

where μ stands for the reduced electron-hole effective mass and r_B stands for the exciton Bohr radius.

Finally, the S_{11} exciton relative motion wave function for the $1S$ state reads

$$\varphi(r) = \frac{1}{\sqrt{r_B}} \exp(-|r|/r_B), \qquad (3)$$

which gives in the k space:

$$\phi_k = 2\sqrt{\frac{r_B}{L}} \frac{1}{1 + (r_B k)^2}, \qquad (4)$$

where L stands for the length of the nanotube so that $\sum_k |\phi_k|^2 = 1$.

A. Reduction of oscillator strength

The PSF contribution to the reduction of oscillator strength for a total number of excitons N is obtained following Ref. [14]:

$$f_0 \propto \sum_{k,k'} \phi_k^* \phi_{k'} \rightarrow f \propto \sum_{k,k'} \phi_k^* (1 - N|\phi_{k'}|^2)\phi_{k'}, \qquad (5)$$

which yields up to first order in the exciton density n:

$$\left.\frac{\Delta f}{f_0}\right|_{PSF} = -N \frac{\sum \phi_k^3}{\sum \phi_k} = -\frac{3}{2} r_B n. \qquad (6)$$

Beyond phase-space filling, an important consequence of the presence of excitons arises from the Coulomb interaction. To first order in perturbation theory, the Coulomb term gives a modification of the exciton wave function, which in turn leads to an additional contribution to the change of oscillator strength of the excitonic transition. We obtain

$$\left.\frac{\Delta f}{f_0}\right|_{EWR} = \frac{1}{\sum \phi_k} \sum_{k'} \frac{\langle 1S|H - H_0|k'\rangle}{-\left(E_b + \frac{\hbar^2 k^2}{2\mu}\right)} + \text{c.c.} \qquad (7)$$

where $|1S\rangle = \sum_k \phi_k |k\rangle$ and c.c. stands for the complex conjugate. The calculation yields

$$\left.\frac{\Delta f}{f_0}\right|_{EWR} = -\frac{N}{E_b \sum \phi_k} \sum_{k,k'} \frac{V_{k,k'}(\phi_k^3 - \phi_k^2 \phi_{k'})}{1 + \frac{\hbar^2 k^2}{2\mu E_b}} + \text{c.c.} \qquad (8)$$

$$= -r_B n. \qquad (9)$$

Finally, the total reduction of oscillator strength reads

$$\left.\frac{\Delta f}{f_0}\right|_{tot} = \left.\frac{\Delta f}{f}\right|_{PSF} + \left.\frac{\Delta f}{f}\right|_{EWR} = -\frac{5}{2} r_B n. \qquad (10)$$

B. Energy shift

To first order in perturbation theory, this Coulomb interaction can be treated in the Hartree-Fock approximation and leads to an energy shift of the excitonic transition that can be calculated as follows:

$$\Delta E = E - E_0 = \langle 1S|H - H_0|1S \rangle \tag{11}$$

$$= \sum_{k,k'} \phi_k^* \langle k|H - H_0|k' \rangle \phi_{k'}, \tag{12}$$

where

$$\langle k|H - H_0|k' \rangle = -\delta_{k,k'} \sum_{k''} V_{kk''} N|\phi_{k''}|^2 + V_{kk'} N|\phi_k|^2. \tag{13}$$

Using the contact interaction approximation [Eq. (1)], yields

$$\Delta E = \frac{U}{2} n = E_b r_B n. \tag{14}$$

C. Broadening

Exciton-exciton scattering results in a global broadening of the lines. This exciton collisional broadening consists of two contributions, namely, the EEA and the EES [9]. In the former process, the collision between two S_{11} excitons results in the annihilation of one of them, whereas the second one is promoted in a higher level. This process is responsible for the exciton population decay observed in time-resolved measurements (Sec. III). This reduced population lifetime automatically results in a minimum broadening of the line given by $(\hbar/n)(dn/dt)$. Using the proportionality between the reduction of oscillator strength $\Delta f/f_0$ and the exciton population [Eq. (10)], we estimated this contribution by numerically computing the quantity $(f_0/\Delta f)[d(\Delta f/f_0)/dt]$ from the data of Fig. 3. In the case of the S_{11} transition, we found that the broadening induced by the diffusion-limited Auger scattering reaches a maximum of 0.2 meV in the first picosecond and remains below 0.02 meV for delays larger than 5 ps. This EEA induced broadening is much smaller than the experimentally observed broadening (Figs. 3 and 4). Therefore, we conclude that EEA brings a negligible contribution to the global broadening.

In the EES process the dephasing of the S_{11} transition results from quasielastic intraband exciton-exciton scattering [15] [Fig. 5(a)]. This scattering rate can be calculated in a self-consistent way until it remains small with respect to the natural linewidth of the transition. This is always the case in our experimental conditions where $\Gamma_0 \simeq 25$ meV, while $\Delta\Gamma \leqslant 5$ meV. Following Ref. [9], we obtain

$$\Delta\Gamma_{EES} = 2 E_b r_B n \xi(b), \tag{15}$$

where $\xi(b) = \frac{4}{\pi} b \int dq \frac{|I(q)|^2}{1+b^2 q^4}$ and $|I(q)| = \frac{16}{(q^2+4)^2} - \frac{6}{(q^2+4)(q^2+1)}$, with $b = \hbar^2/(8\mu r_B \Gamma)$. For $E_b = 350$ meV, giving $r_B = 1.5$ nm, and $\Gamma \simeq \Gamma_0 = 25$ meV, we find $\xi(b) = 0.71$. In total, the overall broadening reads

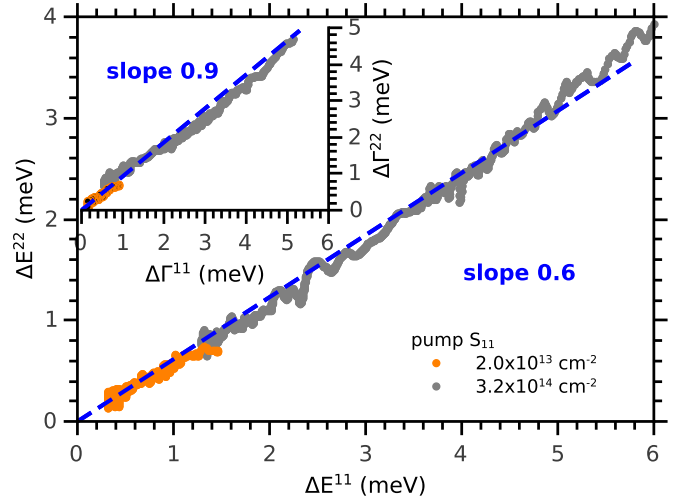$$\Delta\Gamma = 1.4 E_b r_B n. \tag{16}$$

FIG. 6. (Color online) Energy shift of the S_{22} excitonic transition as a function of the one observed on the S_{11} transition for a resonant pumping of the S_{11} transition and for two excitation densities. Inset: broadening of the S_{22} excitonic transition as a function of the one observed on the S_{11} transition for a resonant pumping of the S_{11} transition and for the same excitation densities.

D. Comparison with experiments

We first note that our theoretical approach is based on a first order perturbative theory which leads to corrections that are linear in exciton density. These corrections may, however, be nonlinear in pump intensity since the photocreated population may result from nonlinear population decay mechanisms (such as Auger processes, for instance). Since the evaluation of the exciton population is always indirect, we rather choose to work with ratios of nonlinear quantities (such as energy shift and broadening, for instance) in order to eliminate this exciton density. Importantly, the fact that we observe a linear behavior (see Figs. 4 and 6) means that the first order approximation is sufficient. Quantitatively, we estimate that the exciton density we reach in the present experiments never exceeds 10% of the Mott density $1/r_B$, which ensures that second order corrections are at least one order of magnitude weaker than the main contribution.

We first discuss the nonlinear shift of the excitonic resonances. Importantly, this correction mainly results from the exchange interaction and always gives a blueshift of the excitonic transition. This effect is usually suppressed in three-dimensional materials due to the long-range screening which is no longer efficient in reduced dimensionality. This prediction is in striking agreement with our experimental observations that consistently show a blueshift whatever the excitation density or wavelength.

The most convenient way to make a quantitative comparison between the theoretical predictions and the experimental results is to compare the energy shift to the relative reduction of oscillator strength (Fig. 4). By doing so, we can eliminate the exciton density and the saturation density $(1/r_B)$, both of which are difficult to assess accurately. The only free parameter in this comparison is the exciton binding energy. This latter is known from previous experimental studies based on two-photon fluorescence spectroscopy [2,34] and is

of the order of 350 meV. Importantly, this value is highly sensitive to the microscopic dielectric surrounding of the nanotube, but the sample of the present study and that of Refs. [2,34] are very similar in this respect. Finally, we obtain from our measurements the constant ratio $\frac{\Delta E^{11}/E_b}{\Delta f^{11}/f_0} \simeq -0.13 \pm 0.01$, whereas the theoretical prediction yields -0.4. Thus, theory and experiment agree within a factor of 3, which is satisfactory in terms of order of magnitude. Several reasons can explain the residual discrepancy. Obviously, screening (that was neglected in our calculation) would redshift the transition, which would reduce the predicted blueshift and bring it closer to our observations. However, as already discussed above we do not anticipate this effect to be strong for excitons in a confined geometry. Another possibility would be that some of the excitons split into free electron-hole pairs through exciton-exciton collision, leading to much stronger screening [31,35,36]. In the same time, it was predicted that such electron-hole plasma would enhance the reduction of oscillator strength when the temperature is much lower than the exciton binding energy, which is the case for carbon nanotubes [14]. Another limitation of the model above lies in the contact interaction approximation that may overestimate the short-range interaction at the expense of the long ones, leading again to a global overestimate of the blueshift.

Regarding broadening, our measurements give the constant ratio $\frac{\Delta \Gamma/E_b}{\Delta f/f_0} \simeq -0.05 \pm 0.01$ (cf. inset of Fig. 4), whereas the theoretical prediction yields -0.57 [Eqs. (10) and (16)]. Similarly to the blueshift effect, the absence of screening of interactions by electron-hole pairs may explain the excessive theoretical value for the broadening. In addition, we note that the contact interaction approximation yields an underestimate of the excitonic Bohr radius [37], which in turn leads to an overestimate of the EES broadening. For instance, if we allow the Bohr radius to reach 2.5 nm, in agreement with several experimental reports [9,38], we obtain $\Delta \Gamma = 0.45 E_b r_B n$ and thus $\frac{\Delta \Gamma/E_b}{\Delta f/f_0} \simeq 0.2$ in agreement with the experimental observations within a factor of 4.

V. INTERSUBBAND TRANSITIONS

In agreement with previous reports [8,13,31], we observe a nonlinear signal at the S_{22} transition upon resonant excitation of the S_{11} transition. Remarkably, we show that this signal consists of energy shift and broadening contributions only. The absence of oscillator strength reduction of the S_{22} transition after 1 ps shows that there is no significant population created on S_{22} upon S_{11} excitation. As we shall see in the following sections, energy shift and collisional broadening may arise from intersubband processes. In contrast, such intersubband processes do not give rise to any significant change of oscillator strength. Getting back to the model of Sec. IV, we observe that the PSF contribution vanishes for such intersubband processes since the probed excitonic states (S_{22}) are not built from the states populated by the S_{11} excitons. In addition, the EWR contribution to the reduction of oscillator strength is also strongly reduced for intersubband processes due to the denominator proportional to the energy difference [14]. We thus expect this contribution to be five to ten times smaller

than in the intraband case, in agreement with the experimental results.

This absence of a sizable S_{22} population does not conflict with the $1/\sqrt{t}$ decay law that implies a bimolecular exciton-exciton annihilation and possibly upper bands population through Auger up-conversion, but rather shows that the coupling between the upper and the lower subbands through phonon emission is so fast that the resulting population on S_{22} remains negligible. This is consistent with previous experimental studies [27,28] showing an intersubband coupling rate on the order of 20 ps^{-1}.

A. Energy shift

The nonlinear signal observed on the S_{22} transition results only from interactions between S_{11} excitons photocreated by the pump and S_{22} excitons photocreated by the probe. These interactions lead to energy renormalization and collisional broadening through the same many-body mechanisms that give rise to similar signatures on S_{11}. Indeed, Fig. 6 shows a striking proportionality between the shifts of the upper and the lower exciton, with a proportionality factor of 0.6. A very similar behavior is observed for the broadening (Fig. 6, inset) with a proportionality factor of 0.9, showing that the scattering probability of an S_{22} exciton onto an S_{11} exciton is almost equal to that of the scattering between two S_{11} excitons. Note that although these intersubband energy shift and broadening values are almost as large as the intraband ones, there is no contradiction with the ten times smaller signal observed at the S_{22} resonance: this simply stems from the much larger width of this resonance, which weakens the change of absorption induced by these shifts and broadenings and from the absence of reduction of oscillator strength for intersubband processes.

We developed a simple extension of the model presented in the previous section to account for this effect. We recall that the S_{22} exciton is predominantly built from states belonging to the second conduction and valence subbands of the nanotubes and are therefore distinct from those used to build the S_{11} exciton. In order to compute the spectral shift, we generalize the approach developed by Parks *et al.* [39] in the case of two-dimensional structures. We again consider a contact interaction potential and we restrict our calculations to the 1s states of both the S_{11} and the S_{22} excitons. Their envelope wave functions ϕ_k^{11} and ϕ_k^{22} are thus identical [Eq. (3)] except for the value of the Bohr radius. Following the calculations of Refs. [39,40], we obtain

$$\Delta E^{22} = -\frac{1}{2}\left(R^{S_{22}}_{S_{22}S_{11}S_{11}} + R^{S_{22}}_{S_{11}S_{22}S_{11}}\right)n_{11} \tag{17}$$

with

$$R^{\mu}_{\gamma_1\gamma_2\gamma_3} = \sum_{k,k'} V_{kk'}\left[\phi_k^{\mu}\phi_{k'}^{\gamma_1}\phi_k^{\gamma_2}\phi_k^{\gamma_3} - \phi_{k'}^{\mu}\phi_k^{\gamma_1}\phi_{k'}^{\gamma_2}\phi_{k'}^{\gamma_3}\right]. \tag{18}$$

This expression can be developed in the case of a contact interaction potential neglecting the dielectric screening effects [40]. We obtain

$$\Delta E^{22} = n_{11}\frac{U}{2}\sum_{k,k'}\left[-\left(\phi_{k'}^{22}\right)^2\left(\phi_k^{11}\right)^2 + \phi_k^{22}\phi_{k'}^{22}\left(\phi_{k'}^{11}\right)^2\right.$$
$$\left. - \phi_k^{11}\phi_k^{22}\phi_{k'}^{11}\phi_{k'}^{22} + \phi_k^{11}\phi_{k'}^{11}\left(\phi_{k'}^{22}\right)^2\right]. \tag{19}$$

Remarkably, the sum equals 1, leading to the simple result

$$\Delta E^{22} = n_{11} \frac{U}{2} = \Delta E^{11}. \qquad (20)$$

This remarkably simple result shows that within the contact interaction approximation, the energy shifts of the S_{22} and S_{11} bands induced by the presence of S_{11} excitons are identical. This is in good qualitative agreement with our experimental observation of a linear relationship between the shifts with a proportionality factor of 0.6.

B. Broadening

One of the strong results of this study is the fact that the S_{22} transition is broadened when a population of S_{11} excitons is created. Quantitatively, this crossed broadening is almost equal to the direct one, that is, the one observed on the S_{11} transition itself (see inset of Fig. 6). This crossed broadening is reminiscent of the crossed energy shift described in the previous paragraph. Actually, as in the intraband case, the intersubband broadening can be understood within the framework of collisional broadening [Fig. 5(b)] [15]. Qualitatively, the wave functions of the excitons belonging to different subbands differ only by the extension of the bound relative motion along the tube axis and by a subband-dependent circumferential phase (related to the pseudoangular momentum) [41]. However, the matrix element of the Coulomb interaction is insensitive to the phase factors (the angular momentum is conserved separately for each exciton in either intraband or crossed scatterings since in both cases pictured in Fig. 5 the carriers do not change subband). In addition, since the exciton binding energies are very similar for the S_{11} and S_{22} bands, the envelopes of the exciton wave functions have a similar spatial extension, leading to quasiunity wave-function overlap [37]. In total, although the numerical outcome of the matrix elements of the Coulomb interaction may differ slightly in the intraband and intersubband cases, they both rely on the same selection rules, leading to similar overall collision probabilities in agreement with the experimental observations.

VI. CONCLUSION

In this study, we have conducted a thorough analysis of the nonlinear absorption spectrum of a (6,5) enriched suspension of carbon nanotubes by using a broadband detection scheme covering the first and second excitonic bands. By using intrinsic analysis methods (moment analysis) that do not require any assumption about the line shape, we were able to describe quantitatively the nonlinear spectra with only three elementary deformations of the linear spectrum, namely, a reduction of oscillator strength, an energy shift, and a broadening of the lines. In turn, these generic quantities were connected to a microscopic many-body model involving phase space filling and Coulomb interactions. Importantly, we have shown that the best way to compare this model to the experimental data, is to handle ratios of two of the elementary deformations in order to eliminate the influence of the exciton density, which is always difficult to assess experimentally. In particular, these results clarify the origin of the bleaching of the second exciton (S_{22}) upon pumping the first one. We demonstrate that this bleaching originates from energy shift and broadening contributions only, ruling out the creation of a significant population in the S_{22} level. In fact, we show that intersubband Coulomb interactions play a key role in the nonlinear properties of carbon nanotubes, showing up as collisional broadening between excitons belonging to different subbands or energy shifts subsequent to the presence of excitons in lower subbands. Importantly, we have shown both experimentally and theoretically that the magnitude of these intersubband processes is comparable to the intraband ones, leading to strong intersubband coupling in the nonlinear spectra of carbon nanotubes.

[1] S. Reich, C. Thomsen, and J. Maultzsch, *Carbon Nanotubes: Basic Concepts and Physical Properties* (Wiley-VCH, Weinheim, 2004).

[2] F. Wang, G. Dukovic, L. E. Brus, and T. F. Heinz, Science **308**, 838 (2005).

[3] C. Voisin, S. Berger, S. Berciaud, H. Yan, J.-S. Lauret, G. Cassabois, P. Roussignol, J. Hone, and T. F. Heinz, Phys. Status Solidi B **249**, 900 (2012).

[4] F. Wang, G. Dukovic, E. Knoesel, L. E. Brus, and T. F. Heinz, Phys. Rev. B **70**, 241403 (2004).

[5] L. Colombier, J. Selles, E. Rousseau, J. S. Lauret, F. Vialla, C. Voisin, and G. Cassabois, Phys. Rev. Lett. **109**, 197402 (2012).

[6] S. M. Santos, B. Yuma, S. Berciaud, J. Shaver, M. Gallart, P. Gilliot, L. Cognet, and B. Lounis, Phys. Rev. Lett. **107**, 187401 (2011).

[7] A. Martinez and Z. Sun, Nat. Photonics **7**, 842 (2013).

[8] T. Koyama, S. Yoshimitsu, Y. Miyata, H. Shinohara, H. Kishida, and A. Nakamura, J. Phys. Chem. C **117**, 20289 (2013).

[9] D. T. Nguyen, C. Voisin, P. Roussignol, C. Roquelet, J. S. Lauret, and G. Cassabois, Phys. Rev. Lett. **107**, 127401 (2011).

[10] D. J. Styers-Barnett, S. P. Ellison, B. P. Mehl, B. C. Westlake, R. L. House, C. Park, K. E. Wise, and J. M. Papanikolas, J. Phys. Chem. C **112**, 4507 (2008).

[11] Y.-Z. Ma, C. D. Spataru, L. Valkunas, S. G. Louie, and G. R. Fleming, Phys. Rev. B **74**, 085402 (2006).

[12] H. Zhao, S. Mazumdar, C.-X. Sheng, M. Tong, and Z. V. Vardeny, Phys. Rev. B **73**, 075403 (2006).

[13] Z. Zhu, J. Crochet, M. S. Arnold, M. C. Hersam, H. Ulbricht, D. Resasco, and T. Hertel, J. Phys. Chem. C **111**, 3831 (2007).

[14] S. Schmitt-Rink, D. S. Chemla, and D. A. B. Miller, Phys. Rev. B **32**, 6601 (1985).

[15] C. Ciuti, V. Savona, C. Piermarocchi, A. Quattropani, and P. Schwendimann, Phys. Rev. B **58**, 7926 (1998).

[16] P. M. Vora, X. Tu, E. J. Mele, M. Zheng, and J. M. Kikkawa, Phys. Rev. B **81**, 155123 (2010).

[17] F. Vialla, E. Malic, B. Langlois, Y. Chassagneux, C. Diederichs, E. Deleporte, P. Roussignol, J.-S. Lauret, and C. Voisin, Phys. Rev. B **90**, 155401 (2014).

[18] A. V. Naumov, S. Ghosh, D. A. Tsyboulski, S. M. Bachilo, and R. B. Weisman, ACS Nano **5**, 1639 (2011).

[19] S. A. Kovalenko, A. L. Dobryakov, J. Ruthmann, and N. P. Ernsting, Phys. Rev. A **59**, 2369 (1999).

[20] D. Stich, F. Späth, H. Kraus, A. Sperlich, V. Dyakonov, and T. Hertel, Nat. Photonics **8**, 139 (2013).

[21] J. Allam, M. T. Sajjad, R. Sutton, K. Litvinenko, Z. Wang, S. Siddique, Q.-H. Yang, W. H. Loh, and T. Brown, Phys. Rev. Lett. **111**, 197401 (2013).

[22] M. Hoyuelos and H. O. Mártin, Phys. Rev. E **48**, 3309 (1993).

[23] D. Ben-Avraham and S. Redner, Phys. Rev. A **34**, 501 (1986).

[24] F. Wang, Y. Wu, M. S. Hybertsen, and T. F. Heinz, Phys. Rev. B **73**, 245424 (2006).

[25] B. Yuma, S. Berciaud, J. Besbas, J. Shaver, S. Santos, S. Ghosh, R. B. Weisman, L. Cognet, M. Gallart, M. Ziegler, B. Hönerlage, B. Lounis, and P. Gilliot, Phys. Rev. B **87**, 205412 (2013).

[26] K. Litvinenko, D. Birkedal, V. G. Lyssenko, and J. M. Hvam, Phys. Rev. B **59**, 10255 (1999).

[27] J. S. Lauret, C. Voisin, G. Cassabois, C. Delalande, P. Roussignol, O. Jost, and L. Capes, Phys. Rev. Lett. **90**, 057404 (2003).

[28] C. Manzoni, A. Gambetta, E. Menna, M. Meneghetti, G. Lanzani, and G. Cerullo, Phys. Rev. Lett. **94**, 207401 (2005).

[29] O. A. Dyatlova, C. Koehler, P. Vogel, E. Malic, R. M. Jain, K. C. Tvrdy, M. S. Strano, A. Knorr, and U. Woggon, Phys. Rev. B **90**, 155402 (2014).

[30] D. Hulin, A. Mysyrowicz, A. Antonetti, A. Migus, W. T. Masselink, H. Morkoc, H. M. Gibbs, and N. Peyghambarian, Phys. Rev. B **33**, 4389 (1986).

[31] G. Soavi, F. Scotognella, D. Brida, T. Hefner, F. Spth, M. R. Antognazza, T. Hertel, G. Lanzani, and G. Cerullo, J. Phys. Chem. C **117**, 10849 (2013).

[32] *Many-Particle Physics,* edited by G. D. Mahan (Springer, New York, 2000).

[33] G. Manzke, K. Henneberger, and V. May, Phys. Status Solidi B **139**, 233 (1987).

[34] J. Maultzsch, R. Pomraenke, S. Reich, E. Chang, D. Prezzi, A. Ruini, E. Molinari, M. S. Strano, C. Thomsen, and C. Lienau, Phys. Rev. B **72**, 241402 (2005).

[35] Y. Kumamoto, M. Yoshida, A. Ishii, A. Yokoyama, T. Shimada, and Y. K. Kato, Phys. Rev. Lett. **112**, 117401 (2014).

[36] W. H. Knox, R. L. Fork, M. C. Downer, D. A. B. Miller, D. S. Chemla, C. V. Shank, A. C. Gossard, and W. Wiegmann, Phys. Rev. Lett. **54**, 1306 (1985).

[37] V. Perebeinos, J. Tersoff, and P. Avouris, Phys. Rev. Lett. **92**, 257402 (2004).

[38] L. Lüer, S. Hoseinkhani, D. Polli, J. Crochet, T. Hertel, and G. Lanzani, Nat. Phys. **5**, 54 (2008).

[39] A. M. Parks, M. M. Dignam, and D. Wang, Phys. Rev. B **87**, 205306 (2013).

[40] A. M. Parks, Ph.D. thesis, Queen's University, 2011.

[41] B. O. Tayo and S. V. Rotkin, Phys. Rev. B **86**, 125431 (2012).